Metal-electrode-free Window-like Organic Solar Cells with p-doped Carbon Nanotube Thin-film Electrodes

Il Jeon[1], Clement Delacou[2], Antti Kaskela[3], Esko I. Kauppinen[3], Shigeo Maruyama[2,4], and Yutaka Matsuo[1,*]

1: Department of Chemistry, School of Science, The University of Tokyo, 7-3-1 Hongo, Bunkyo-ku, Tokyo 113-0033, Japan

2: Department of Mechanical Engineering, School of Engineering, The University of Tokyo, 7-3-1 Hongo, Bunkyo-ku, Tokyo 113-8656, Japan

3: Department of Applied Physics, Aalto University School of Science, 15100, FI-00076 Aalto, Finland

4: National Institute of Advanced Industrial Science and Technology (AIST), 1-2-1 Namiki, Tsukuba, 305-8564, Japan

Correspondence and requests for materials should be addressed to Y.M. (email: matsuo@chem.s.u-tokyo.ac.jp).

ABSTRACT:

Broad applications along with flexibility and low-cost is the main feature of organic solar cells. Transparent organic solar cells have been reported in great numbers emphasizing this point. Success of transparent organic solar cells hinges on full transparency, high power conversion efficiency, and low cost fabrication. Recently, carbon-based nanotubes and graphene, which meet those criteria, have emerged as transparent conductive electrodes. However, their usage as a top electrode has been limited due to mechanical difficulties in fabrication and doping. Here expensive top metal electrode was replaced by highly performing and easy-to-transfer aerosol-synthesized carbon nanotubes to produce transparent organic solar cells. Moreover, the carbon nanotubes were doped by two new methodologies presented in this work: HNO_3 doping 'Sandwich transfer' and MoO_x thermal doping 'Bridge transfer'. While both doping methods enhanced the performance of the carbon nanotubes, thus photovoltaic performance in device, HNO_3 doping Sandwich method with 4.1% power conversion efficiency was marginally more effective than the Bridge transfer with a power conversion efficiency of 3.4%. Applying much thinner carbon nanotube film with 90% transparency decreased the efficiency little, yet still retained to 3.7%. Compared with the efficiency of the non-transparent metal-based solar cells (7.8%), it showed more than 50% efficiency while being largely transparent. The doping methodologies proposed in this work are not only limited to carbon nanotubes but also any carbon-based electrodes. Moreover the top electrode application of carbon-based electrodes proposed here is viable in other types of solar cells, including perovskite solar cells.

Organic solar cells (OSCs) have drawn great attention over other competing solar cell technologies owing to low-cost, high efficiency, and diverse applications.[1–3] Current progress in power conversion efficiency (PCE) of OSCs has reached around 10% amounting both

tandem and non-tandem architectures, demonstrating promising future of OSCs as solar energy harvesters.[4,5] In addition to the pursuit of high efficiency, OSCs have also been intensively studied for their potential in making advances for broader applications.[6,7] On the same note, future OSCs are regarded to be greener technology that serves various functions such as wearable, surface conforming, window application. Prerequisites to these include use of metal-free, mechanically resilient, and translucence materials, while retaining a high PCE. The first step towards this achievement is replacing metal electrode, which is expensive and blindingly glare. Previously, many attempts have been made in demonstrating transparent and flexible solar cells such as building-integrated photovoltaics and solar chargers for portable electronics using metallic grids, nanowire networks, metal oxides, or conducting polymers.[8–20] Yet, transparent conductors often result in either low visible light transparency, low PCEs, or low flexibility, because no suitable transparent and conductive material was adopted in device design and fabrication.

Single-walled carbon nanotubes (SWNTs) are regarded to accomplish the aforementioned shortcomings for their mechanical flexibility, abundant carbon composition, facile synthesis, and direct roll-to-roll processability.[21] SWNTs are structurally the simplest class of carbon nanotubes with typical diameters in the range of 0.4–3.0 nm.[22] Following the discoveries by Iijima in early 1990s, its development has been continued and now the high quality free-standing purely single-walled carbon nanotubes show the transparency of over 90% with the resistance of around 85 Ω/sq.[23] Use of this conductive SWNT films as an electrode replacing ITO in photovoltaics has been reported in great numbers.[24,25] However, a SWNT film working as a top-electrode has been rarely reported because of the challenging nature of SWNT lamination from above.[26] There was one recent success in the work presented by Li et al.[26] Their SWNT films were used as the top-electrode in perovskite solar cells.

However, their SWNT films could not be doped, because doping laminated SWNT electrode is extremely difficult without damaging the device.

Here we report SWNT-based metal-free and window-like transparent OSCs where SWNT films have been doped by two mainstream dopants, HNO_3 and MoO_3 which we named 'Sandwich transfer' and 'Bridge transfer', respectively. The HNO_3-doped, and MoO_3-doped 60% transparent SWNT-laminated OSCs showed PCEs of 4.1% and 3.4%, respectively. Applying 90% transparent SWNT films, which rendered tinted-window visual, resulted in PCEs of 3.7% and 3.1% for HNO_3-doped and MoO_3-doped, respectively, while the reference ITO-based OSC showed a PCE of 7.8%. Hence, we introduce window-applicable transparent OSCs by means of safely doping direct- and dry-lamination of SWNT films for the top electrode, bypassing the expensive and energy-consuming metal deposition process. The double-sided light response feature of these transparent yet highly efficient solar cells offers advantages in many applications. We expect the methodologies presented here will open the way to the future of multifunctional OSCs.

Results

Aerosol single-walled carbon nanotubes. The randomly oriented SWNT networks with high purity and long nanotube bundle length were synthesized by the aerosol CVD method.[23,27] The floating catalyst aerosol CVD was carried out in a scaled-up reaction tube with the diameter of 150 mm. The dry deposited SWNT networks had high purity as evidenced by clear Van Hove peaks in UV-vis spectroscopy and relatively low defect derived D band intensity in Raman spectroscopy.[28] Furthermore, as the process required no sonication-based dispersion step, the resulting SWNT network consisted of exceptionally long SWNTs. Facile transferability is another advantage of the Aerosol SWNT films. Once deposited from the

aerosol, the CNTs showed strong tube-to-tube interaction and assembled into a freestanding thin film. The SWNT films were easily peeled off from a nitrocellulose film by a pair of tweezers and transferred onto other substrates for device fabrication.

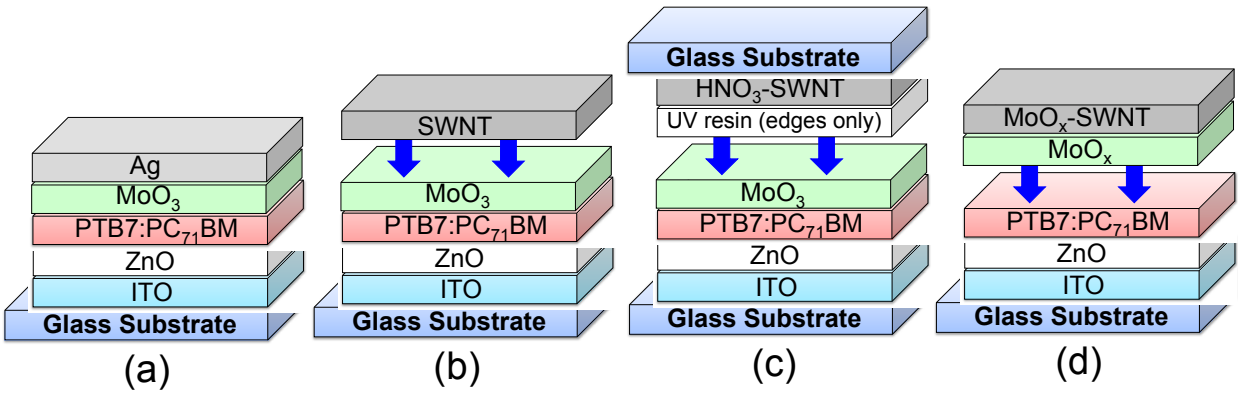

Figure 1. Illustrations of architecture of (a) a conventional inverted OSC, (b) a SWNT-based transparent OSC, (c) a HNO_3-doped SWNT-based transparent OSC, and (d) a MoO_x-doped SWNT-based transparent OSC.

Architectures of the solar cell devices. The structures of SWNT-based transparent OSCs are shown in Figure 1. Figure 1a shows the conventional inverted OSC structure where Ag was used as an anode. This entails expensive metal deposition cost and leads to a non-transparent device. Figure 1b represents the same structure, except that Ag has been replaced by low-cost and highly transparent aerosol SWNT. Here, light can be shone either from ITO or SWNT sides, or both sides to generate photo-induced power. Thus, it can be called window-like transparent OSCs. The conductivity and the transparency of SWNT must be enhanced by doping in order to produce efficiency solar cells. Figure 1c and 1d demonstrate HNO_3-doped, and MoO_x-doped SWNT-applied window-like transparent OSCs, respectively. Due to the difficult nature of doping, two very different methodologies were employed and resulted in different architectures as illustrated. This will be discussed in detail later in this work. It is

worth noting that a mixture of the low bandgap polymer, thieno[3,4-b]64thiophene/benzodithiophene (PTB7) and the acceptor, [6,6]-phenyl C71-butyric acid methyl ester ($PC_{71}BM$) with an additive, 1,8-diiodoctane (DIO) has been used as the photoactive layer for all the devices on account of their high efficiency.

Performance of SWNT-laminated transparent organic solar cells. Photoluminescence quenching can demonstrate the charge extraction ability.[29] A PTB7-based organic photoactive layer was deposited on a glass substrate and a SWNT film was laminated from top. As shown in Figure S2, the spectrum of the organic photoactive layer was suppressed significantly when the SWNT film sat on top of it. This indicates effective charge extraction and successful lamination.

Table 1. Photovoltaic Performance for the SWNT-based transparent inverted OSCs under one sun, AM1.5G illumination (100 mW/cm^2)

Device	Light direction	Anode	Dopant	V_{OC} (V)	J_{SC} (mA/cm^2)	FF	R_S (Ωcm^2)	R_{SH} (Ωcm^2)	PCE_{best} (%)
A	from ITO	Ag	None	0.73	16.0	0.65	16	6.4×10^4	7.8
B	from SWNT	SWNT T=90%		0.58	4.8	0.32	470	4.6×10^5	0.9
C	from ITO			0.66	6.5	0.40	320	8.9×10^4	1.8
D	with reflector			0.66	8.6	0.39	280	5.8×10^4	2.2
E	from ITO	SWNT T=90%	HNO_3	0.69	9.5	0.56	70	1.5×10^4	3.7
F			MoO_x	0.62	8.8	0.56	100	1.8×10^5	3.1
G		SWNT T=60%	HNO_3	0.70	9.0	0.65	53	1.6×10^7	4.1
H			MoO_x	0.68	8.2	0.60	61	8.4×10^5	3.4

Footnote: T = transmittance

First, OSCs using 90% transparent SWNT films were fabricated. Then, PCEs were measured with light shining from the SWNT side, the ITO side, and the ITO side with a mirror reflecting from behind. According to Table 1, different PCEs were obtained depending on

which direction light was coming from (Table 1: Devices B and C). When light was shone from the ITO side, a PCE of 2% was obtained which was approximately twice higher than the PCE when light was shone from the SWNT side (0.9%). These values are substantially low in comparison with the non-transparent conventional reference, Device A (7.8%). This is because the SWNT films were not doped. The UV-vis spectra (Figure S3a) revealed that ITO possessed higher transparency than 90% transparent SWNT. The difference got bigger when we included the whole device: the photoactive layer, ZnO, and MoO_3. As well as the intrinsic transmittance of the layers, the internal surface reflection between layers might also have augmented this difference. In other words, light shining on the ITO side is optically more favored for the solar cell performance. This results in a higher PCE for Device B than that of Device C, for a larger number of photon is converted into higher short-circuit current density (J_{SC}) for Device B. Incident photo to current efficiency (IPCE) was measured to confirm this. As expected, when light was shone from the ITO side, more charges were extracted (Figure S3b).

Regarding the photovoltaic parameters in Table 1, Device B showed not only high J_{SC} but also higher open-circuit voltage (V_{OC}) and higher fill factor (FF) than those of Device C. This is a typical characteristic of solar cells that can be described by the Shockley equation. In principle, it is related to logarithmic scaling of V_{OC} with the light intensity.[30] Therefore, Device C with higher J_{SC} will exhibit higher V_{OC}. Concerning FF, equation (1) shows that FF is affected by V_{OC} too.[31] This is especially so with real solar cell devices which show a non-ideal diode behavior. Thus, low J_{SC} can induce low V_{OC} and FF.

$$FF = \frac{V_{OC} - \ln(V_{OC} + 0.72)}{V_{OC} + 1} \qquad (1)$$

The value of shunt resistance (R_{SH}) is especially important in transparent OSCs because there is not enough light intensity. With low light intensity, both the bias point and the current

of the solar cell devices will decrease. This causes the equivalent resistance of the solar cell devices to approach R_{SH}.[32] If the equivalent and shunt resistances are similar, the fraction of the total current flowing through the R_{SH} will increase and this may lead to recombination of charges. So it is crucial that we have a device system with a high enough R_{SH} value to avoid recombination. From the current-voltage (*J*-*V*) curves shown in Figure 2a and 2b, we can see that 90% transparent SWNT applied OSCs possess sufficiently high R_{SH} regardless of the light direction.

In the conventional OSCs' case, metal electrodes can act as a rear reflector to direct unabsorbed light back to the photoactive layer. This provides a higher photocurrent especially in the wavelength region shorter than 700 nm. However, for the transparent OSCs, because the no light can be reflected back and the active material is not thick enough to absorb all of the sunlight, much light going through unabsorbed. When a silver reflector (mirror) was introduced at the opposite side of the light source, the J_{SC} increased from 6.5 mA/cm^2 to 8.6 mA/cm^2 (Table 1: Device D; Figure 2d). However, despite the enhanced light intensity, V_{OC} and FF did not improve any further. This reveals that the maximum V_{OC} obtained from use of pristine 90% transparent SWNT is limited to around 0.66. We suspect this could be due to imperfect interface contact between SWNT and MoO_3.[33,34] In general, V_{OC} is controlled by difference between highest occupied molecular orbital (HOMO) of a donor and lowest unoccupied molecular orbital (LUMO) of an acceptor; what is more, the HOMO and LUMO are affected by the interfacial layers' Fermi levels and electrodes' work functions.[35] Therefore, in our belief, poor contact between SWNT and MoO_3 was the limiting factor for the V_{OC}. The overall PCE improvement was only 0.4%. This concludes that the double-sided light response feature of the transparent OSCs leads to sufficient photon excitations and that the application of a reflector at the cost of losing window-like transparency is not necessary.

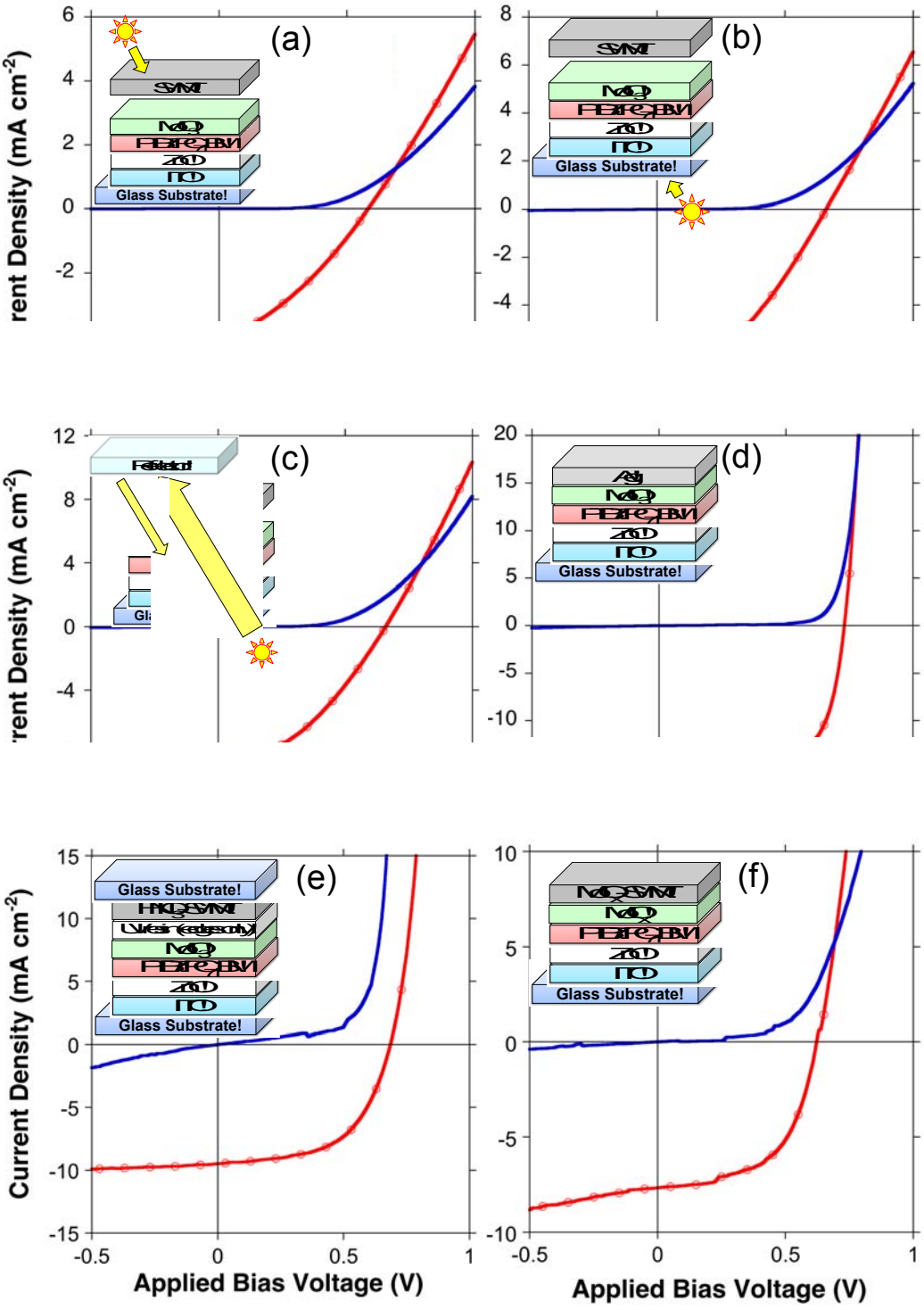

Figure 2. *J-V* curves under one sun (red dotted) and in dark (blue plane) of (a) a SWNT-based transparent OSC with light from the SWNT side, (b) a SWNT-based transparent OSC with light from the ITO side, (c) a SWNT-based transparent OSC with light from the ITO side and a reflector, and (d) a conventional inverted OSC.

Doping methodologies for SWNT-laminated transparent solar cells. Though transparent OSCs have been demonstrated, SWNT should be doped to improve its conductivity and transmittance to boost the PCE. So far, doping SWNT, which is being laminated from top, has not been reported yet. This is owing to mechanical difficulty of the doping: unlike SWNT on a glass substrate, doping the top-laminated SWNT will damage the device underneath. Hence, in this work, we devised two methodologies of safely doping SWNT by HNO_3 and MoO_3 each.

Application of HNO_3(aq) acid has been reported to be one of the most effective doping methods.[36] Nevertheless, its strong acidic nature makes it impossible to apply directly: When a drop of HNO_3 was applied on a SWNT laminated device, it percolated through the film and utterly destroyed the organic materials underneath (Figure S4). Therefore, doping had to be performed on SWNT only first. Figure 3a illustrates how the HNO_3-doped Sandwich-transfer can be proceeded. One droplet of HNO_3 was applied to a SWNT film on a glass substrate followed by heating at 80 °C for 5 min to dry up. The SWNT film turned slightly reddish as the acid dried up and this signified successful doping. The HNO_3-SWNT was then transferred onto a quasi-fabricated OSC interfacing a MoO_3 film like a sandwich. UV resin was applied at the edges only to reinforce the adhesion. A PCE of 3.7% was achieved with the light source positioned at the ITO side (Table 1: Device E). Enhancement in J_{SC} and reduction in series resistance (R_S) confirmed improvement of the transparency and the conductivity of HNO_3-doped SWNT. Increase in V_{OC} meant that the interfacial contact improved. This we surmise is owing to pressure applied on HNO_3-SWNT during the Sandwich-transfer.

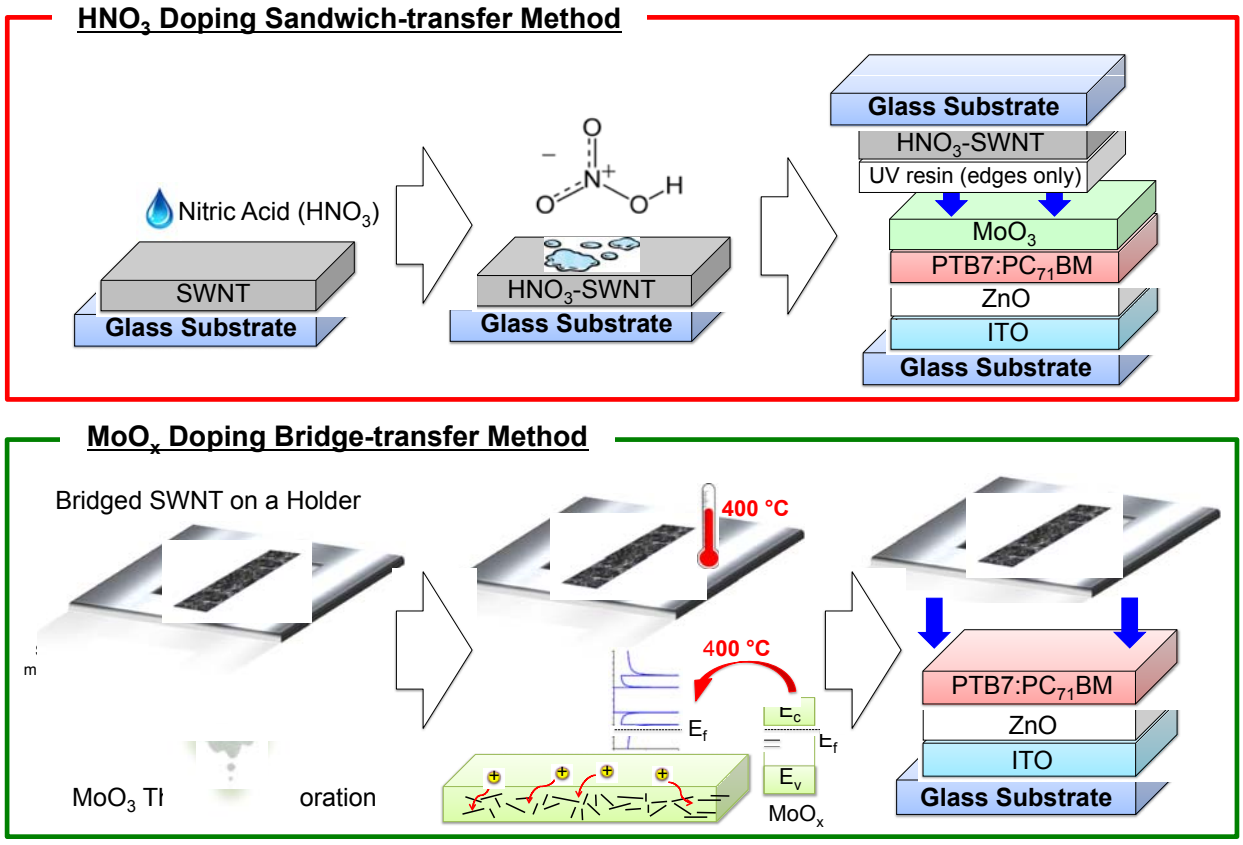

Figure 3. Graphical illustrations of (a) HNO_3 doping Sandwich-transfer process (above) and (b) MoO_x thermal doping Bridge-transfer process (below).

Thermal MoO_x doping of SWNT is known to be more stable doping than HNO_3 in spite of its marginally lower effectiveness.[37] Its successful application in OSCs has been reported.[38] However, again this is not applicable to the SWNT films laminated from top, because it undergoes high temperature annealing process of above 300 °C. Thus, we propose bridge-transfer methodology (Figure 3b). SWNT was transferred onto a metal holder where a SWNT film hung like a bridge (Figure S5). Then a shadow mask was placed below the SWNT film to mask the electrode contact area. MoO_3 was deposited from below through vacuum thermal evaporation. MoO_3-SWNT was then annealed at 400 °C together with the holder to boost the doping effect: MoO_3-SWNT was reduced to MoO_x-SWNT where x is between 2 and 3.[37] MoO_x-SWNT was gently laminated using the holder onto a quasi-fabricated device where the

MoO_3 film was not deposited because the MoO_x on the SWNT can function as both a dopant and electron-transporting layer. A PCE of 3.1% was recorded for this device (Table 1: Device F). Lower J_{SC} and higher R_S than those of Device E were observed because MoO_x thermal doping is known to be less effective than HNO_3 doping. An important point to note in this methodology is that because the SWNT hung precariously on the metal holder, extra caution was necessary during the handling. Any small external impact or draught strong enough to crumple the SWNT created micro-wrinkles on SWNT films, which were invisible to naked eye but only by atomic force microscopy (Figure S6). Lower V_{OC} in this device possibly came from two reasons: The first reason is the remnants of mirco-wrinkles undermining the interface. Second reason is that pressure was not applied during the lamination of SWNT unlike the Sandwich-transfer method. Compared to the HNO_3-SWNT Sandwich-transfer, this method manifested lower reproducibility due to sensitive process.

Despite high PCEs, both doping methodologies suffered from instability with *J*-*V* sweeps (Figure 2e and 2f). We ascribe this to the mechanical instability of the fabrication i.e., possible excess pressure applied on SWNT during the HNO_3-SWNT Sandwich-transfer, and delicate nature of the MoO_x-SWNT Bridge-transfer. However, if mechanical optimizations are followed, high efficient and stability will be obtained.

Application of thicker SWNT films. Thicker SWNT films possess higher conductivity, but their transmittance is lower. By incorporating the thicker SWNT films (60% transparency at 550 nm wavelength), higher PCEs were obtained (Figure S7 and S8). HNO_3-doped device produced 4.1% (Table 1: Device G) and MoO_x-doped device produced 3.4% (Table 1: Device H). Arising from the higher conductivity of the 60%-SWNT films, FF was higher than that of the 90%-SWNT-based devices by around 0.1. Interestingly, V_{OC} of Device H was higher than expected. We attribute this to thicker SWNT films being less vulnerable to

the micro wrinkle formation during the Bridge-transfer. Despite lower transmittance of the films, both Device G and H displayed rather high J_{SC}, because the main source of photon comes from the ITO side not the SWNT side. While it may appear obvious to employ thicker SWNT to gain higher PCEs, using them will substantially undermine the window-like visual of transparent OSCs (Figure S9). The improvement of PCE only came in the expense of window-like transparency.

Discussion

Non-doped SWNT (90% transmittance)-based MoO_3/PTB7:$PC_{71}BM$:DIO/ZnO/ITO window-like transparent OSCs showed a PCE of 1.8%. Aerosol synthesized SWNT electrode, which was laminated from above as a top-electrode showed facile processability, chemical stability, electrical compatibility, and mechanical resilience. By applying p-doping on SWNT through HNO_3 Sandwich-transfer and MoO_3 Bridge-transfer methods, both of which are unprecedented, PCEs of the transparent OSCs further improved to 3.7% and 3.1%, respectively. Obtaining an even higher PCE of 4.1% was possible at the cost of transparency by incorporating thicker SWNT films. By replacing metal electrodes, these OSCs showed advantageous properties of low cost, window-like transparency, and glare-free visuals. This research successfully demonstrated a promising potential in window solar cell applications and flexible tandem OSCs.

Methods

Aerosol SWNT Preparation. SWNT was synthesized by an aerosol (floating catalyst) CVD method based on ferrocene vapor decomposition in a CO atmosphere. The catalyst

precursor was vaporized by passing ambient temperature CO through a cartridge filled with ferrocene powder. The flow containing ferrocene vapor was then introduced into the high-temperature zone of a ceramic tube reactor through a water-cooled probe and mixed with additional CO. To obtain stable growth of SWNT, a controlled amount of CO_2 was added together with the carbon source (CO). SWNT was directly collected downstream of the reactor by filtering the flow through a nitrocellulose or silver membrane filter (Millipore Corp., USA; HAWP, 0.45 μm pore diameter).

Device Fabrication. For the reference device, ITO substrates with size 15 × 15 mm^2 and an active area of 3 × 3 mm^2 with a sheet resistance of 6 Ω/square (Kuramoto Co., Ltd.) were sonicated in cleaning surfactant (Semi Clean, M-Lo), water, acetone and 2-isopropanol for 15 minutes each. The substrates were then dried in an oven at 70 °C. ITO substrates were exposed to UV/O_3 for 30 min in order to remove any remaining organic impurities. They were transferred to a nitrogen filled glovebox for further fabrication.

ZnO sol–gel films were prepared using the method reported by Heeger et al.[39] The metal oxides were baked at 200 °C before depositing the photoactive layer.

For the photoactive layer deposition, PTB7 and $PC_{71}BM$ were purchased from Luminescence Technology Corporation and used as received without further purification. A blend solution of PTB7 and $PC_{71}BM$ was prepared in a mixed solvent of chlorobenzene (99%, CB) and DIO at a 97:3 ratio. PTB7 (10 mg) and $PC_{71}BM$ (15 mg) were initially dissolved in CB inside a nitrogen glovebox (0.97 mL). The solution was left stirring overnight at 60 °C. After 24 h, the corresponding amount of DIO (30 μL) was added. The new solution was stirred 1 h at 70 °C. The solution of PTB7:$PC_{71}BM$:DIO (80 nm) was spin-coated at 1500 rpm for 60 s on ZnO layer to give approximately 100 nm. Hole-transporting layer, MoO_3 was deposited on top, under vacuum via a thermal evaporator. 15 nm MoO_3 was deposited with the average

rate of 0.2 Å/s. To improve the contact between the solar simulator and SWNT, Ag (100 nm) pattern was deposited only at the contact where wires of the solar simulator will be clipped.

Transfer of non-doped SWNT. SWNT films were transferred onto MoO_3 by laminating from the top. A drop of poly(3,4-ethylenedioxythiophene)/poly(styrenesulfonate) (PEDOT:PSS) was applied and spin-coating at 4500 rpm for 60 s to assist lamination.

Transfer of HNO_3-doped SWNT by 'Sandwich transfer method'. SWNT films were transferred on bare glass substrates. HNO_3 (70% in water) was applied drop-wise and dried at 80°C to dope the SWNT films. The HNO_3-doped SWNT substrates were transferred onto MoO_3 and Ag patterned device (MoO_3/PTB7:$PC_{71}BM$:DIO/ZnO/ITO) like a sandwich and UV-resin was applied at the edges only in order to hold the two substrates and encapsulate.

Transfer of MoO_x-doped SWNT by 'Bridge transfer method'. A special holder for SWNT films was prepared and SWNT films were transferred onto the holder so that the films hang like a bridge. 15 nm MoO_3 was thermally deposited on the bridged SWNT films followed by thermal annealing at 300 °C for 3 h anaerobically to induce MoO_x doping. The bridged SWNT films were transferred carefully on to the Ag patterned photoactive layer. A drop of PEDOT:PSS was applied and spin-coating at 4500 rpm for 60 s to assist lamination. Since MoO_x can function as the HTL, MoO_3 step was omitted for this method only. In other words, SWNT/MoO_x was laminated on PTB7:$PC_{71}BM$:DIO/ZnO/ITO rather than MoO_3/PTB7:$PC_{71}BM$:DIO/ZnO/ITO.

Characterizations. Current-voltage (*J*–*V*) characteristics were measured by software-controlled source meter (Keithley 2400) in dark conditions and 1 sun AM 1.5G simulated sunlight irradiation (100 mW/cm^2) using a solar simulator (EMS-35AAA, Ushio Spax Inc.), which was calibrated using a silicon diode (BS-520BK, Bunkokeiki). Topography images were recorded using an AFM operating in tapping mode (SPI3800N, SII). SEM measurement was

carried out on S-4800 (Hitachi). inVia Raman microscope (Renishaw) were used for the Raman measurement. Shimadzu UV-3150 was used for the UV-vis-NIR measurement.

References

1. Yu, G., Gao, J., Hummelen, J. C., Wudl, F. & Heeger, A. J. Polymer Photovoltaic Cells: Enhanced Efficiencies via a Network of Internal Donor-Acceptor Heterojunctions. *Science* **270,** 1789–1791 (1995).
2. Dennler, G., Scharber, M. C. & Brabec, C. J. Polymer-Fullerene Bulk-Heterojunction Solar Cells. *Adv. Mater.* **21,** 1323–1338 (2009).
3. Li, G., Zhu, R. & Yang, Y. Polymer solar cells. *Nat. Photonics* **6,** 153–161 (2012).
4. Ameri, T., Li, N. & Brabec, C. J. Highly efficient organic tandem solar cells: a follow up review. *Energy Environ. Sci.* **6,** 2390 (2013).
5. Chen, J.-D. *et al.* Single-Junction Polymer Solar Cells Exceeding 10% Power Conversion Efficiency. *Adv. Mater.* **27,** 1035–1041 (2015).
6. Lipomi, D. J., Tee, B. C.-K., Vosgueritchian, M. & Bao, Z. Stretchable Organic Solar Cells. *Adv. Mater.* **23,** 1771–1775 (2011).
7. Park, H. J., Xu, T., Lee, J. Y., Ledbetter, A. & Guo, L. J. Photonic Color Filters Integrated with Organic Solar Cells for Energy Harvesting. *ACS Nano* **5,** 7055–7060 (2011).
8. Henemann, A. BIPV: Built-in solar energy. *Renew. Energy Focus* **9,** 14–19 (2008).
9. Zhu, R., Kumar, A. & Yang, Y. Polarizing Organic Photovoltaics. *Adv. Mater.* **23,** 4193–4198 (2011).
10. Bailey-Salzman, R. F., Rand, B. P. & Forrest, S. R. Semitransparent organic photovoltaic cells. *Appl. Phys. Lett.* **88,** 3–5 (2006).
11. Ng, G.-M. *et al.* Optical enhancement in semitransparent polymer photovoltaic cells. *Appl. Phys. Lett.* **90,** 103505 (2007).
12. Huang, J., Li, G. & Yang, Y. A Semi-transparent Plastic Solar Cell Fabricated by a Lamination Process. *Adv. Mater.* **20,** 415–419 (2008).

13. Lee, Y.-Y. *et al.* Top Laminated Graphene Electrode in a Semitransparent Polymer Solar Cell by Simultaneous Thermal Annealing/Releasing Method. *ACS Nano* **5,** 6564–6570 (2011).

14. Ameri, T. *et al.* Fabrication, Optical Modeling, and Color Characterization of Semitransparent Bulk-Heterojunction Organic Solar Cells in an Inverted Structure. *Adv. Funct. Mater.* **20,** 1592–1598 (2010).

15. Gaynor, W., Lee, J.-Y. & Peumans, P. Fully Solution-Processed Inverted Polymer Solar Cells with Laminated Nanowire Electrodes. *ACS Nano* **4,** 30–34 (2010).

16. Colsmann, A. *et al.* Efficient Semi-Transparent Organic Solar Cells with Good Transparency Color Perception and Rendering Properties. *Adv. Energy Mater.* **1,** 599–603 (2011).

17. Lunt, R. R. & Bulovic, V. Transparent, near-infrared organic photovoltaic solar cells for window and energy-scavenging applications. *Appl. Phys. Lett.* **98,** 113305 (2011).

18. Meiss, J., Holzmueller, F., Gresser, R., Leo, K. & Riede, M. Near-infrared absorbing semitransparent organic solar cells. *Appl. Phys. Lett.* **99,** 193307 (2011).

19. Bauer, A., Wahl, T., Hanisch, J. & Ahlswede, E. ZnO:Al cathode for highly efficient, semitransparent 4% organic solar cells utilizing TiO_x and aluminum interlayers. *Appl. Phys. Lett.* **100,** 073307 (2012).

20. Xia, X. *et al.* Infrared-transparent polymer solar cells. *J. Mater. Chem.* **20,** 8478 (2010).

21. De Volder, M. F. L., Tawfick, S. H., Baughman, R. H. & Hart, A. J. Carbon Nanotubes: Present and Future Commercial Applications. *Science* **339,** 535–539 (2013).

22. Hatton, R. A., Miller, A. J. & Silva, S. R. P. Carbon nanotubes: a multi-functional material for organic optoelectronics. *J. Mater. Chem.* **18,** 1183 (2008).

23. Kaskela, A. *et al.* Aerosol-Synthesized SWCNT Networks with Tunable Conductivity and Transparency by a Dry Transfer Technique. *Nano Lett.* **10,** 4349–4355 (2010).

24. Du, J., Pei, S., Ma, L. & Cheng, H. M. 25th anniversary article: carbon nanotube- and graphene-based transparent conductive films for optoelectronic devices. *Adv. Mater.* **26,** 1958–1991 (2014).

25. Jeon, I. *et al.* Single-Walled Carbon Nanotube Film as Electrode in Indium-Free Planar Heterojunction Perovskite Solar Cells: Investigation of Electron-Blocking Layers and Dopants. *Nano Lett.* **15,** 6665–6671 (2015).

26. Li, Z. *et al.* Laminated Carbon Nanotube Networks for Metal Electrode-Free Efficient Perovskite Solar Cells. *ACS Nano* **8,** 6797–6804 (2014).

27. Nasibulin, A. G. *et al.* Multifunctional Free-Standing Single-Walled Carbon Nanotube Films. *ACS Nano* **5,** 3214–3221 (2011).

28. Cui, K. *et al.* Air-stable high-efficiency solar cells with dry-transferred single-walled carbon nanotube films. *J. Mater. Chem. A* **2,** 11311–11318 (2014).

29. Docampo, P., Ball, J. M., Darwich, M., Eperon, G. E. & Snaith, H. J. Efficient organometal trihalide perovskite planar-heterojunction solar cells on flexible polymer substrates. *Nat. Commun.* **4,** 2761 (2013).

30. Koster, L. J., Mihailetchi, V. D., Ramaker, R. & Blom, P. W. M. Light intensity dependence of open-circuit voltage of polymer:fullerene solar cells. *Appl. Phys. Lett.* **86,** 123509 (2005).

31. Green, M. A. Solar cell fill factors: General graph and empirical expressions. *Solid. State. Electron.* **24,** 788–789 (1981).

32. Bunea, G., Wilson, K., Meydbray, Y., Campbell, M. & De Ceuster, D. Low Light Performance of Mono-Crystalline Silicon Solar Cells. in *2006 IEEE 4th World Conference on Photovoltaic Energy Conference* **2,** 1312–1314 (IEEE, 2006).

33. Cravino, A. Origin of the open circuit voltage of donor-acceptor solar cells: Do polaronic energy levels play a role? *Appl. Phys. Lett.* **91,** 243502 (2007).

34. Qi, B. & Wang, J. Open-circuit voltage in organic solar cells. *J. Mater. Chem.* **22,** 24315 (2012).

35. Steim, R., Kogler, F. R. & Brabec, C. J. Interface materials for organic solar cells. *J. Mater. Chem.* **20,** 2499 (2010).

36. Shin, D. W. *et al.* A role of HNO_3 on transparent conducting film with single-walled carbon nanotubes. *Nanotechnology* **20,** 475703 (2009).

37. Hellstrom, S. L. *et al.* Strong and Stable Doping of Carbon Nanotubes and Graphene by MoO_x for Transparent Electrodes. *Nano Lett.* **12,** 3574–3580 (2012).

38. Jeon, I. *et al.* Direct and Dry Deposited Single-Walled Carbon Nanotube Films Doped with MoO_x as Electron-Blocking Transparent Electrodes for Flexible Organic Solar Cells. *J. Am. Chem. Soc.* **137,** 7982–7985 (2015).

39. Kyaw, A. K. K. *et al.* Efficient Solution-Processed Small-Molecule Solar Cells with Inverted Structure. *Adv. Mater.* **25,** 2397–2402 (2013).

Acknowledgements

This work was supported by the Grants-in-Aid for Scientific Research (15H02219), IRENA project by JST-EC DG RTD, and Strategic International Collaborative Research Program, SICORP. Part of this work was supported by the Strategic Promotion of Innovative Research and Development, Japan Science and Technology Agency (JST). I.J. appreciates Japan Student Services Organization.

Author contributions

Y.M. and I.J. designed the project, with assistance in supervision from E.K. S.M. provided advice throughout the project I.J. conceived and carried out the experiments. I.J. and Y.M. wrote the manuscript. I.J., C.D. performed the measurements. A.K. synthesized, and provided SWCNTs for the experiments.

Additional information

Supplementary Information accompanies this paper at http://www.nature.com/naturecommunications

Competing financial interests: The authors declare no competing financial interests.